Solid State Communications 168 (2013) 1–5

Contents lists available at SciVerse ScienceDirect

Solid State Communications

journal homepage: www.elsevier.com/locate/ssc

Vortex flux pinning mechanism and enhancement of in-field J_c in succinic acid doped MgB_2

S.R. Ghorbani [a,*], M. Darini [c], X.L. Wang [b], M.S.A. Hossain [b], S.X. Dou [b]

[a] Department of Physics, Ferdowsi University of Mashhad, Mashhad, Iran
[b] Institute for Superconducting and Electronic Materials, University of Wollongong, Wollongong, New South Wales 2522, Australia
[c] Department of Physics, Hakim Sabzevari University, Sabzevar, Iran

ARTICLE INFO

Article history:
Received 13 March 2013
Received in revised form
5 June 2013
Accepted 13 June 2013
by P. Chaddah
Available online 21 June 2013

Keywords:
A. Succinic acid doped MgB_2
D. Critical current density
D. Flux pinning mechanism

ABSTRACT

The field dependence of the resistivity and the critical current density, $J_c(B)$, of MgB_2 doped with 10 wt% wet and dry succinic acid have been investigated by magnetic measurements. The dry succinic acid significantly enhanced the upper critical field, the irreversibility field, and the $J_c(B)$ compared to the wet succinic acid doped MgB_2 and the pure MgB_2. The field dependence of $J_c(B)$ was analyzed within the collective pinning model. The observed temperature dependence of the crossover field, $B_{sb}(T)$, from the single vortex to the small vortex bundle pinning regime shows that flux pinning arising from variation in the critical temperature, δT_c, is the dominant mechanism for the wet sample over the whole studied temperature range, while there is a competition between δT_c pinning and the pinning from variation in the mean free path, δl, for the dry sample.

1. Introduction

MgB_2 superconductor has been regarded as a promising superconductor for industrial applications due to its large coherence length (ξ), simple crystal structure, low material cost, and high critical current density (J_c) compared to other superconductors [1,2]. Despite these advantages the critical current density of MgB_2 decreases rapidly in high magnetic field because of its poor flux pinning. Therefore, research approaches have been directed towards either improving J_c by improving grain connectivity, or improving in-field performance by different methods.

The current-density decay behavior is governed by the pinning mechanism. The two main types of pinning centers in this alloy are intergrain boundaries and point defect centers [3,4]. Vortices and pinning centers mostly interact with each other through the magnetic interaction and the core interaction. The former interaction is based on the proximity effect, i.e., contact between superconductor and non-superconductor surfaces, and the latter is due to the variation in the superconducting order parameter.

An effective method to improve the J_c is to introduce flux pinning centers into MgB_2 by means of chemical dopants. Many elements and compounds have been used as dopants [5–11]. Results have shown that carbon and its derivatives are the best doping agents in MgB_2 due to substitution of carbon for boron. The purity and size of the B powder may play an important role in determining the properties of the MgB_2 [12]. To improve these properties, the ball-milling method is interesting, as it allows size control of the starting material because C and its derivatives with small dimensions can easily be reacted with B for MgB_2 superconductor formation. It was also found [13] that substitution of the roughly 10 wt% carbon derived media showed the highest level of C-substitution, x in the formula $Mg(B_{1-x}C_x)_2$, and then it seemed to be saturated when doping level increased. This means that 10 wt% is enough for C-substitution, in spite of the gradually increased amount. There has been no study as yet on the effects of dry and wet carbon derived media on the superconductivity properties of doped MgB_2, however.

Non-superconductor particles give rise to two important core mechanisms: δT_c pinning and δl pinning. The δT_c pinning results from the random distribution of spatial variations in the transition temperature, and the δl pinning arises from charge-carrier mean free path variations [14,15].

We have studied the effects of dry and wet carbon derived media, such as succinic acid ($C_4H_6O_4$), on the superconducting properties of MgB_2. It was found that a significant flux-pinning enhancement in MgB_2 can be easily achieved by doping with succinic acid ($C_4H_6O_4$). Our results showed that the C released from the decomposition of the $C_4H_6O_4$ is substituted into B sites. The inclusion of the succinic acid leads to a reduction in the lattice parameters, as well as in T_c and the residual resistance ratio (RRR: $R(300\,K)/R(40\,K)$), resulting in a significant enhancement of $J_c(H)$, the irreversibility field, H_{irr}, and the upper critical field, H_{c2}.

* Corresponding author. Tel./fax: +98 511 8796983.
E-mail addresses: sh.ghorbani@um.ac.ir, srezagho@yahoo.com (S.R. Ghorbani).

0038-1098/$ - see front matter © 2013 Elsevier Ltd. All rights reserved.
http://dx.doi.org/10.1016/j.ssc.2013.06.010

2. Experiment

Two samples of doped MgB_2 with 10 wt% succinic acid were synthesized by the in-situ method. In the first sample, the boron and succinic acid were mixed together and were sintered at 210 °C. Then, the resultant powder was mixed with magnesium and was fired at 900 °C for 30 min (dry sample). In the second sample, toluene was also added to the boron and succinic acid in the first step to achieve greater homogeneity of the sample (wet sample). The details of the sample preparation are given in Ref. [9]. The X-ray diffraction (XRD) patterns of the compound were collected by using Cu Kα radiation.

Magnetic and transport measurements were performed using a physical properties measurement system (PPMS; Quantum Design). The critical current density was calculated by using the Bean approximation, $J_c = 20\Delta M/Va(1-a/3b)$, where a and b are the width and the length of the sample perpendicular to the applied field, respectively, with $a \le b$, V is the sample volume, and ΔM is the height of the M–H hysteresis loop, which were measured over the temperature range of 20–34 K for both samples.

3. Results and discussion

Fig. 1 shows the X-ray diffraction (XRD) patterns for the doped and undoped samples. Although the XRD results revealed that all samples were crystallized in the MgB_2 structure as the major phase, a few impurity lines of MgO were observed. A minor amount of MgO is present in all the samples. The (100) peak is slightly shifted towards higher angles, indicating a decrease in the a lattice parameter. The (002) peak reflects the c lattice parameter. The position of this peak does not change noticeably, and consequently, c does not change.

The lattice parameters were calculated from the XRD patterns. For the pure sample, a and c were 3.085 and 3.526 Å, while a was 3.058 Å and 3.071 Å for the wet and the dry samples, respectively, and c was 3.517 Å for both samples. The decrease in lattice parameter a is quite pronounced, while the c-parameter is constant. The change in this lattice parameter confirms the partial replacement of boron by carbon. The level of C substitution, x in the formula $Mg(B_{1-x}C_x)_2$, can be estimated as $x = 7.5 \times \Delta(c/a)$, where $\Delta(c/a)$ is the change in c/a compared to a pure sample [16]. It was found that the x value was 0.065 and 0.029 for the wet and the dry samples, respectively, suggesting that C substitution on B sites for the wet sample was larger than for the dry sample. These observations were further explained by the T_c values, to be discussed later.

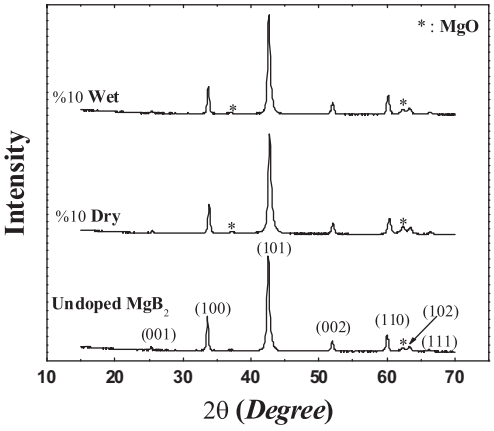

Fig. 1. XRD patterns of undoped and succinic acid-doped MgB_2.

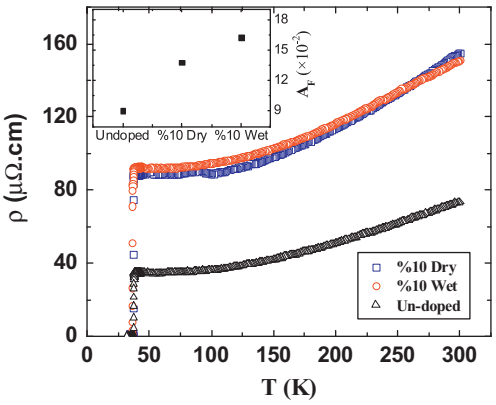

Fig. 2. Electrical resistivity ρ vs. temperature T for the undoped MgB_2, and the 10 wt% dry and wet $C_4H_6O_4$ doped samples sintered at 900 °C. Inset: connectivity factor A_F for all samples.

Fig. 2 shows the resistivity versus temperature curves (ρ–T) over the temperature range from 30 to 300 K. The resistivity at 40 K increased from 34.9 μΩ cm for the pure MgB_2 to 88.5 and 92.5 μΩ cm for the dry and wet doped MgB_2, respectively. The T_c values and residual resistivity ratios, $R(300\,K)/R(40\,K)$ (RRR), were obtained to be 37.83 K, 36.59 K, and 37.23 K; and 2.12, 1.77, and 1.63, for the pure sample and for the wet and dry $C_4H_6O_4$–MgB_2 samples, respectively. Therefore, the large variation in the residual resistivity and the reduced RRR values indicate that the intraband scattering rates are enhanced in the samples with the addition of $C_4H_6O_4$. The obtained T_c results show that the T_c was decreased by the succinic acid doping, in agreement with the decreasing a lattice parameter, suggesting different C level substitution on the B sites. These results are in agreement with the correlation between the C substitution level and both T_c and a, as demonstrated by Kazakov et al. [17]. They found that the superconducting transition temperature and the a lattice parameter decreased monotonically with increasing carbon content in $Mg(B_{1-x}C_x)_2$ single crystals with $0 \le x \le 0.10$, with a faster decrease for $x > 0.10$.

The connectivity factor, A_F, from the relation $A_F = \Delta\rho_{sc}/\Delta\rho$, where $\Delta\rho_{sc}$ is the single crystal resistivity and $\Delta\rho = \rho(300\,K) - \rho(40\,K)$, from our experimentally measured resistivity, was also evaluated by Rowell analysis [18]. We observed that the A_F values of the both the dry and the wet $C_4H_6O_4$ doped samples were larger than that of the undoped MgB_2 reference sample. As can be seen in inset of Fig. 2, the A_F values are 0.09, 0.14, and 0.16 in the undoped MgB_2, and the dry and wet $C_4H_6O_4$–doped MgB_2, respectively. The high A_F of the wet sample is due to the use of toluene, which improves the homogeneity and the connectivity of the sample. The dry $C_4H_6O_4$ doped MgB_2 sample has small connectivity and what appear to be inhomogeneous grains, but the A_F values of all samples are still lower than the ideal value of 1. This indicates that there are some obstacles to current, such as voids or MgO impurities, for all the samples.

The H_{c2} and H_{irr} were determined from the 90% or 10% drop, respectively, at the transition in the normal-state resistivity values in the R–T curves. The H_{c2} and H_{irr} results as a function of normalized temperature T/T_c are shown in Figs. 3 and 4. The R–T curves are shown in the insets of Figs. 3 and 4 for the 10 wt% dry and wet $C_4H_6O_4$ doped MgB_2, respectively. The H_{c2} and H_{irr} values of the undoped sample are also included in Figs. 3 and 4 for comparison. The upper critical field value at 25 K for the undoped sample was about 7 T, while the values for the wet and the dry samples at the same temperature were 7.3 T and 8.7 T, respectively. The above results reveal that although the wet $C_4H_6O_4$ doped MgB_2 shows improved H_{c2} and H_{irr} values compared to the undoped sample, the dry $C_4H_6O_4$ doped MgB_2 shows the most

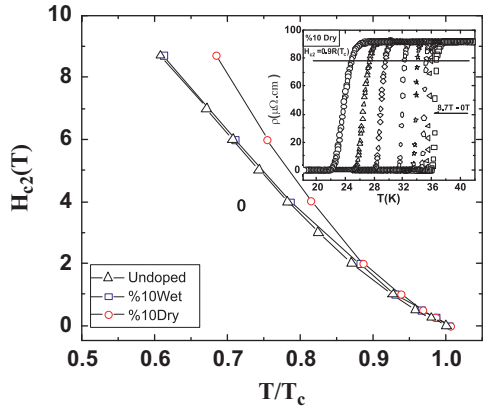

Fig. 3. H_{c2} versus reduced temperature for the undoped MgB_2, and the 10 wt% dry and wet succinic acid doped samples. Inset: $\rho(T)$ curves for the dry sample.

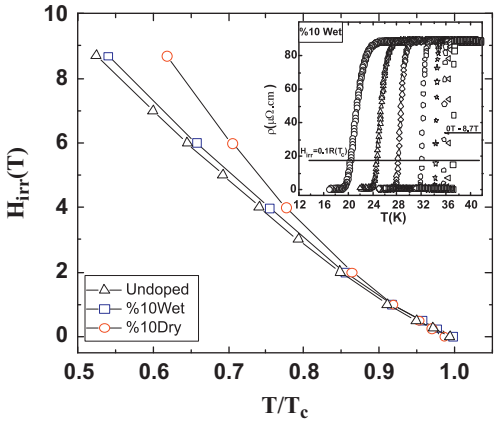

Fig. 4. H_{irr} versus reduced temperature for the undoped MgB_2, and the 10 wt% dry and wet succinic acid doped samples. Inset: $\rho(T)$ curves for the wet sample.

significant enhancement. The dry $C_4H_6O_4$ doped MgB_2 shows a further reduction in the residual resistance ratio (RRR) compared with that for the wet $C_4H_6O_4$ doped MgB_2 sample, resulting in further enhanced H_{c2} and H_{irr} values due to reduced scattering length (the mean free path, l). In addition, the inclusion of the $C_4H_6O_4$ in the doped MgB_2 results in two effects. The first is the partial substitution for B by C released from the $C_4H_6O_4$, which may induce disorder on the lattice sites and result in the enhancement of the H_{irr} and H_{c2}. The second effect is that the nonreactive C can introduce point defects and affect the grain boundaries without any substitution effect. Both effects reduce the mean free path, l, which can lead to enhancement of the H_{irr} and H_{c2}. The latter effect may be responsible for the significantly enhanced H_{irr} and H_{c2} for the dry $C_4H_6O_4$ doped MgB_2 compared to the wet sample.

Magnetic hysteresis loops were collected in the temperature range of 5, and 20–32.5 K for both the wet and the dry 10 wt% succinic acid doped MgB_2 samples. The critical current density was calculated by using the Bean critical model. Fig. 5 shows the magnetic field dependence of the J_c for both doped MgB_2 samples at different temperatures. For comparison purposes, the data from the pure MgB_2 sample at 5 and 20 K are also included in the figure. The J_c at 5 and 20 K for both the dry and the wet $C_4H_6O_4$–MgB_2 samples at high fields is higher than for the pure MgB_2 sample, which was made under the same conditions as the $C_4H_6O_4$-MgB_2. As can be seen from Fig. 5, the J_c is very much enhanced in high magnetic fields for both the dry and the wet $C_4H_6O_4$–MgB_2 samples, and it is more than 10 times higher than for the undoped

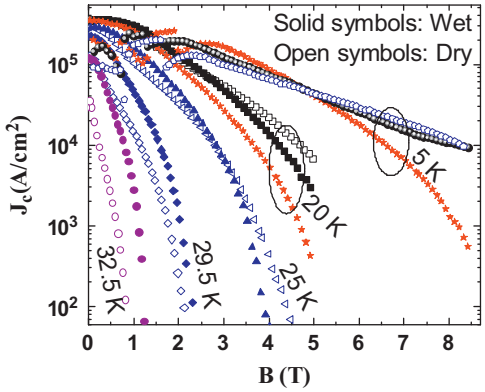

Fig. 5. Magnetic field dependence of the critical current density J_c for the wet and dry 10 wt% succinic acid doped MgB_2. The solid star symbols show the J_c of the pure MgB_2 sample at 20 K.

MgB_2 at $T=5$ K and $B=8$ T. Therefore, the $C_4H_6O_4$ doped MgB_2 exhibits significantly improved pinning in high fields over a wide temperature range compared with the undoped MgB_2 sample. At $T=5$ and 20 K and in lower magnetic fields, however, the J_c of the $C_4H_6O_4$ doped samples is lower than that of the undoped sample. The O in the $C_4H_6O_4$ doping can easily react with Mg to form MgO, which is responsible for two effects. The first one is that the amount of MgB_2 phase is accordingly decreased, which decreases the effective superconducting volume inside the $C_4H_6O_4$ doped samples. This effect results in decreased J_c in low fields. The second effect is the formation of nanosized pinning centers, which improves J_c–H behavior in high magnetic fields.

The J_c of the wet sample is larger than that of the dry sample at high temperature over the entire range of magnetic field. At temperatures lower than 25 K at higher magnetic field, the dry sample exhibits significantly better J_c. This is because at low magnetic field, the effective area is the dominant factor for the J_c, and as can be seen in the inset of Fig. 2, the wet sample has a larger A_F than the dry sample. As mentioned above, the dry $C_4H_6O_4$ doped MgB_2 sample has small connectivity and what appear to be inhomogeneous grains. The connectivity of the wet sample was improved, however, and the grain morphology was more refined and more homogeneous. This indicates that there is degradation of the crystallinity of the dry sample due to the nonreactive C in between grain boundaries, resulting in the introduction of point defects. Flux pinning by point defects is the dominant factor for J_c at high magnetic field, however. Therefore, more pinning centers were introduced by the dry $C_4H_6O_4$ doped MgB_2 sample than the wet sample, which resulted in better $J_c(B)$ performance at high magnetic fields and lower temperatures.

To study the pinning properties of succinic acid doped MgB_2, the volume pinning force $F_p = J_c \times B$ was calculated for both samples. The magnetic field dependence of the normalized pinning force ($f=F_p/F_{p,max}$), where $F_{p,max}$ is the maximum values of F_p, is shown in the inset of Fig. 6. As can be seen, the width and the maximum position of the $f(B)$ curves depend on temperature. A broader curve indicates higher pinning strength. The scaling behavior for the normalized volume pinning force $f_p=F/F_{p,peak}$, was examined for $b=B/B_{peak}$, where B_{peak} is the magnetic field at the maximum of F_p. The results are shown in Fig. 6. The $f_p(b)$ curve does not exhibit scaling behavior at higher temperatures. Otherwise, scaling was achieved by fitting with δT_c pinning, $f=(9/4)b(1-b^2)$, and correlated pinning, $f=(25/16)b^{1/2}(1-b/5)^2$, which was inferred by Higuchi et al. [19]. The fitting results are shown by the solid and dashed curves in Fig. 6(a) and (b). In lower fields, the experimental data are in good agreement with the δT_c pinning mechanism for both wet and dry samples. At normalized magnetic fields larger than b_{max} and at the temperature of 32.5 K, flux

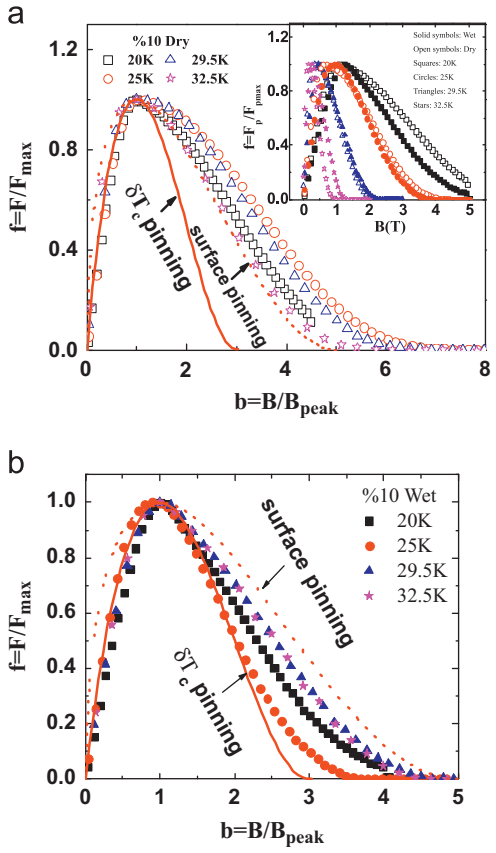

Fig. 6. Magnetic field dependence of the reduced pinning force $f(b)$ for the temperature range of 20–32.5 K for (a) dry and (b) wet 10 wt% succinic acid doped MgB_2. The solid and dashed curves show fittings to two different types of point pinning centers. The solid and dashed curves represent $f=(9/4)b(1-b^2)$ and $f=(25/16)b^{1/2}(1-b/5)^2$, respectively, for the two different pinning mechanisms. The inset to (a) shows the normalized pinning force vs. $B(T)$ for the wet and dry doped samples at different temperatures.

pinning is dominated by correlated pinning for the dry sample, while at $T<32.5$ K, the experimental data does not fit either of these models. For the wet sample, the experimental data are located between the theoretical curves for correlated pinning and δT_c pinning. Therefore, we cannot obtain any dominant pinning mechanism.

According to the collective theory [20], J_c is field independent at magnetic fields lower than the crossover field, B_{sb}, which marks the transition from the single vortex to the small bundle pinning regime. Below this regime, single vortex pinning governs the vortex lattice:

$$B_{sb}\propto J_{sv}B_{c2}, \tag{1}$$

where J_{sv} is the critical current density in the single vortex pinning regime. At higher fields, $B>B_{sb}$, $J_c(B)$ decreases quickly, and it follows an exponential law:

$$J_c(B)\approx J_c(0)exp[-(B/B_0)^{3/2}], \tag{2}$$

where B_0 is a normalization parameter on the order of B_{sb}. At higher magnetic fields, a power dependence in the form of $J_c\propto B^{-\beta}$ acts from B_{sb} up to another crossover field, B_{lb} (to the large bundle pinning regime).

For clarification, $-\log[J_c(B)/J_c(B=0)]$ as a function of B is shown in a double logarithmic plot in the inset of Fig. 7 for the dry sample at 25 K. It shows clearly that Eq. (2) well describes the experimental data for intermediate fields, while deviations from the fitting curves can be observed at both low and high fields. The deviation at fields smaller than B_{sb} is associated with crossover

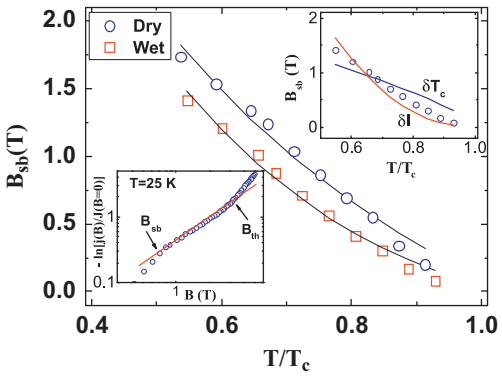

Fig. 7. Temperature dependence of B_{sb}, with solid lines showing the fit to Eq. (4). Inset (lower): double logarithmic plot of $-\ln[J_c(B)/J_c(0)]$ as a function of B at $T=25$ K. The crossover fields B_{sb} and B_{th} are indicated by arrows. Inset (upper): The δT_c and δl pinning curves correspond to Eq. (3) for the dry sample.

from the single-vortex-pinning regime to the small-bundle-pinning regime. The high-field deviation that is very close to the irreversibility line could be related to large thermal fluctuations. The crossover field to this deviation is denoted as B_{th}. Large-bundle pinning does not fit our data. The obtained crossover field B_{sb} is shown in Fig. 7 as a function of temperature for both dry and wet samples. The B_{sb} displays different trends for the two samples, which indicates different vortex pinning mechanisms.

Two main reasons for the T_c fluctuation are the partial substitution of C for B and Mg deficiency, which lead to a broad T_c distribution in the sample [21], while the grain boundaries and inclusions cause mean free path fluctuation and hence the δl pinning. Griessen et al. [22] determined the δT_c pinning and the δl pinning mechanisms by considering the different temperature dependences of the critical current density, J_{sv}, in the single vortex pinning regime. For δT_c pinning, $J_{sv}\propto(1-t^2)^{7/6}(1+t^2)^{5/6}$ with $t=T/T_c$, while for the case of δl pinning,. $J_{sv}\propto(1-t^2)^{5/2}(1+t^2)^{-(1/2)}$. In the single-vortex-pinning region the following B_{sb} temperature dependence can be obtained [14]:

$$B_{sb}=B_{sb}(0)\left(\frac{1-t^2}{1+t^2}\right)^{\nu}, \tag{3}$$

where the parameter $\nu=0.67$ and 2 for δT_c and δl pinning, respectively.

The curves of $B_{sb}(T)$ for δT_c and δl pinning were fitted to the data, as shown in the upper inset of Fig. 7. As is clear from Fig. 5, there is no agreement between our experimental data and Eq. (3) with $\nu=2$ and 0.67, and that strongly suggests that the δT_c and the δl pinning mechanisms coexist in our samples.

To investigate the real pinning mechanism of the doped MgB_2 samples, the B_{sb} data was analyzed within the following expression:

$$B_{sb}=P_1B_{sb}^{T_c}+P_2B_{sb}^{l}, \tag{4}$$

where $B_{sb}^{T_c}$ and B_{sb}^{l} are the expressions for δT_c and δl pinning, respectively. P_1 and P_2 are fitting parameters. The B_{sb} data obtained from $J_c(B)$ was well described by Eq. (4), as shown by the solid curves in Fig. 7. In order to compare the effects of the δT_c and the δl pinning mechanisms, the P parameter was defined as $P_{T_c}=P_1B_{sb}^{T_c}/B_{sb}$ or $P_l=P_2B_{sb}^{l}/B_{sb}$, which represent δT_c or δl pinning effects, respectively. The results of both pinning effect contributions are shown in Fig. 8. The trends in both δT_c pinning and δl pinning are stable for both dry and wet 10 wt% succinic acid doped MgB_2 samples, while the actual values of the pinning contribution are dependent on the samples. This is because the partial C substitution on the B sites and inclusions in between grain boundaries are different for the dry and wet $C_4H_6O_4$ doped MgB_2 samples. As can be seen in Fig. 8, the δT_c pinning is the dominant

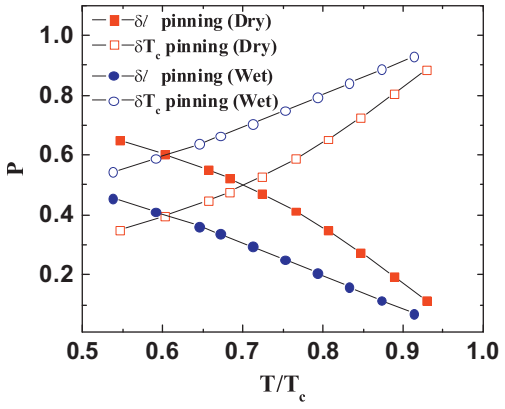

Fig. 8. δT_c and δl pinning contributions as functions of reduced temperature.

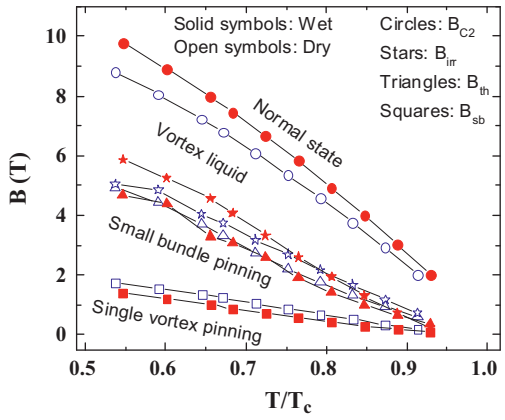

Fig. 9. Magnetic phase diagram for the dry and the wet samples.

mechanism for the wet sample over the whole studied temperature range. For the dry sample, there is a competition between δT_c pinning and δl pinning. δl pinning is the dominant mechanism at low temperature, but with increasing temperature, δl pinning decreases, and δT_c pinning increases. The reduced temperature t_{eq} where both pinning mechanisms have equal effects is 0.7 for the dry sample. These results suggest that the competition between the δT_c and the δl pinning mechanisms is stronger for the dry 10 wt% succinic acid doped MgB_2 sample.

Using the obtained B_{c2} and B_{irr} from the resistance measurements and the derived crossover fields B_{sb} and B_{th} from the critical current results, the reconstructed B–T phase diagram is shown in Fig. 9. According to the collective pinning model [20], the disorder-induced spatial fluctuations in the solid vortex lattice can be clearly divided into markedly different regimes, according to the strength of the applied field. The three distinguishable regimes are: (1) single vortex pinning, which governs the region below B_{sb}; (2) small bundle pinning, which holds between B_{sb} and B_{th}; and (3) the region between B_{th} and B_{irr}, where thermal fluctuations are important.

In conclusion, we observed enhancements in the upper critical field, the irreversibility field, and the critical current density of the succinic acid doped MgB_2. These results provide strong evidence that the dry succinic acid produced very strong pinning centers, which enhanced $J_c(B)$ at high magnetic fields and low temperatures. On comparing with the collective pinning theory, the observed temperature dependence of the crossover field, $B_{sb}(T)$, from the single vortex to the small vortex bundle pinning regime shows that δT_c pinning is the dominant mechanism for the wet sample over the whole studied temperature range, while there is a competition between δT_c pinning and δl pinning for the dry sample. The field-temperature diagram has been drawn, which separates the single vortex pinning, small bundle pinning, and large thermal fluctuation regions.

Acknowledgments

M.S.A.H. acknowledges the support of the Australian Research Council (Grant no. DE130101247).

References

[1] C. Buzea, T. Yamashita, Supercond. Sci. Technol. 14 (2001) R115.
[2] Y. Iwasa, D.C. Larbalestier, M. Okada, R. Penco, M.D. Sumption, X. Xi, Trans. Appl. Supercond. 16 (2006) 1457.
[3] J. Wang, Z.X. Shi, H. Lv, T. Tamegai, Physica C 445 (2006) 462.
[4] S.X. Dou, A.V. Pan, S. Zhou, M. Ionescu, X.L. Wang, J. Horvat, H.K. Liu, P.R. Munroe, Appl. Phys. Lett. 94 (2003) 1850;
I. Pallecchi, C. Tarantini, H.U. Aebersold, V. Braccini, C. Fanciulli, C. Ferdeghini, F. Gatti, E. Lehmann, P. Manfrinetti, D. Marré, A. Palenzona, A.S. Siri, M. Vignolo, M. Putti, Phys. Rev. B 71 (2005) 212507.
[5] S.R. Ghorbani, X.L. Wang, S.X. Dou, Sung-Ik Lee, M.S.A. Hossain, Phys. Rev. B 78 (2008) 184502.
[6] S.X. Dou, S. Soltanian, J. Horvat, X.L. Wang, S.H. Zhou, M. Ionescu, H.K. Liu, P. Munroe, M. Tomsic, Appl. Phys. Lett. 81 (2002) 3419.
[7] W.K. Yeoh, J.H. Kim, J. Horvat, X. Xu, M.J. Qin, S.X. Dou, C.H. Jiang, T. Nakane, H. Kumakura, P. Munroe, Supercond. Sci. Technol. 19 (2006) 596.
[8] H. Yamada, M. Hirakawa, H. Kumakura, H. Kitaguchi, Supercond. Sci. Technol. 19 (2006) 175.
[9] B.J. Senkowicz, J.E. Giencke, S. Patnaik, C.B. Eom, E.E. Hellstrom, D.C. Larbalestier, Appl. Phys. Lett. 86 (2005) 202502.
[10] R.H.T. Wilke, S.L. Bud'ko, P.C. Canfield, D.K. Finnemore, Phys. Rev. Lett. 92 (2004) 217003.
[11] A. Matsumoto, H. Kumakura, H. Kitaguchi, H. Hatakeyama, Supercond. Sci. Technol. 16 (2003) 926.
[12] X. Xu, M.J. Qin, K. Konstantinov, D. Dos Santos, W.K. Yeoh, J.H. Kim, S.X. Dou, Supercond. Sci. Technol. 19 (2006) 466.
[13] M.S.A. Hossain, J.H. Kim, X.L. Wang, X. Xu, G. Peleckis, S.X. Dou, Supercond. Sci. Technol. 20 (2007) 112;
H. Ağıl, Ö. Çiçek, E. Ertekin, A. Motaman, M.S.A. Hossain, S.X. Dou, A. Gencer, J. Supercond. Nov. Magn. 26 (2013) 1525.
[14] M.J. Qin, X.L. Wang, H.K. Liu, S.X. Dou, Phys. Rev. B 65 (2002) 132508.
[15] S.L. Prischepa, M.L. Della Rocca, L. Maritato, M. Salvato, R. Di Capua, M.G. Maglione, R. Vaglio, Phys. Rev. B 67 (2003) 024512.
[16] M. Avdeev, J.D. Jorgensen, R.A. Ribeiro, S.L. Bud'ko, P.C. Canfield, Physica C 387 (2003) 301.
[17] S.M. Kazakov, R. Puzniak, K. Rogack, A.V. Mironov, N.D. Zhigadlo, J. Jun, Ch. Soltmann, B. Batlogg, J. Karpinski, Phys. Rev. B 71 (2005) 024533.
[18] J.M. Rowell, Supercond. Sci. Technol. 16 (2003) R17.
[19] T. Higuchi, S.I. Yoo, M. Murakami, Phys. Rev. B 59 (1999) 1514.
[20] G. Blatter, M.V. Feigelman, V.B. Geshkenbein, A.I. Larkin, V.M. Vinokur, Rev. Mod. Phys. 66 (1994) 1125.
[21] S.X. Dou, O. Shcherbakova, W.K. Yeoh, J.H. Kim, S. Soltanian, X.L. Wang, C. Senatore, R. Flukiger, M. Dhalle, O. Husnjak, E. Babic, Phys. Rev. Lett. 98 (2007) 097002.
[22] R. Griessen, Wen Hai-hu, A.J.J. van Dalen, B. Dam, J. Rector, H.G. Schnack, S. Libbrecht, E. Osquiguil, Y. Bruynseraede, Phys. Rev. Lett. 72 (1994) 1910.